Evolutionary Structure of the Eastern Pacific Double ITCZ Based on Satellite Moisture Profile Retrievals

CHRISTOPHER E. LIETZKE*

Department of Atmospheric Science, Colorado State University, Fort Collins, Colorado

CLARA DESER

Climate and Global Dynamics Division, National Center for Atmospheric Research, Boulder, Colorado

THOMAS H. VONDER HAAR

Department of Atmospheric Science, Cooperative Institute for Research in the Atmosphere, Colorado State University, Fort Collins, Colorado

(Manuscript received 18 June 1999, in final form 23 November 1999)

ABSTRACT

For about a month near the boreal vernal equinox, the eastern Pacific intertropical convergence zone (ITCZ) is observed to form two troughs quasi-symmetrically situated about the equator near 5°–7° latitude during years when an equatorial sea surface cold tongue is present (e.g., La Niña years). The three-dimensional structure and temporal evolution of the eastern Pacific double ITCZ is documented using weekly cloud liquid and ice water fields and relative humidity profiles retrieved from Special Sensor Microwave/Temperature-2 measurements. The depth of convection in the southern branch of the double ITCZ, as determined by the coincident presence of cloud liquid and ice as well as by upward motion inferred from the relative humidity field, is observed to be sensitive to both the underlying SST and subsidence from the northern branch. The equatorial sea surface cold tongue appears to be the determining factor regulating the formation of a double ITCZ in the eastern Pacific. Areas of deep convection within the double ITCZ are accompanied by surface wind convergence maxima. However, the coincident maxima in deep convection and surface convergence are located several degrees of latitude equatorward of the highest sea surface temperatures.

1. Introduction

The earth's climate system is strongly influenced by ocean–atmosphere interaction in the Tropics. The thermally direct Hadley circulation over the tropical oceans is driven by the near-equatorial convergence zones, principally the intertropical convergence zone (ITCZ) and the South Pacific convergence zone. The former is typically a single band of convection located north of the equator for much of the year. During the boreal spring, however, the ITCZ has been observed, in some years, to form in two distinct bands, quasi-symmetrically situated about the equator in the tropical eastern Pacific. Because the southern branch of the double ITCZ occurs in a notoriously data-poor region of the oceans, it was not until the launch of the first experimental meteorological satellites in the 1960s by the Environmental Space Services Administration (ESSA) that its existence was clearly established (Kornfield et al. 1967). Further studies using the ESSA satellites (Hubert et al. 1969; Winston 1971; Gruber 1972; Musk 1976) confirmed that the double ITCZ structure as observed in the cloudiness field, was only present in the eastern Pacific for a limited time during the boreal spring. More recently, Waliser and Gautier (1993) used the Highly Reflective Cloud (Garcia 1985) dataset to document the frequency and intensity of convection in the global ITCZ, including the double ITCZ in the tropical eastern Pacific. Vertical profiles of moisture and temperature in the eastern Pacific ITCZ have been documented by Fernandez-Partagas and Estoque (1985), but only during summer when the ITCZ is located north of the equator. The temporal evolution and vertical structure of the double ITCZ in the eastern Pacific have received little observational study due to the paucity of data.

* Current affiliation: ITT Aerospace/Communications, Fort Wayne, Indiana.

Corresponding author address: Christopher E. Lietzke, ITT Aerospace/Communications, 1919 W. Cook Road, P.O. Box 3700, Fort Wayne, IN 46801-3700.
E-mail: chris.lietzke@itt.com

Numerical modeling studies directed at understanding the spatial structure of tropical convection and hence the position of the ITCZ began in earnest soon after the ESSA observations. Charney (1971) proposed that conditional instability of the second kind (CISK) is responsible for tropical cyclogenesis and the ITCZ. Holton et al. (1971) proposed that the position of the ITCZ is determined by easterly wave propagation, while Lindzen (1974) used wave-CISK theory to assign a latitudinal preference to the ITCZ. Pike (1971) employed an axially symmetric coupled atmosphere–ocean model to investigate the latitudinal preference of the ITCZ based on meridional sea surface temperature (SST) profiles. More recently, Waliser and Somerville (1994) demonstrated, using an axially symmetric primitive equation model, that the ITCZ has a latitudinal preference regardless of where the meridional SST maximum is located. The presence of a double ITCZ year-round is a common error produced by many coupled atmosphere–ocean general circulation models (GCMs; Mechoso et al. 1995). This problem is so pervasive that it is referred to as the coupled GCM ''double ITCZ syndrome'' (Ma et al. 1996).

The purpose of this study is to document the three-dimensional structure and evolution of the double ITCZ in the eastern tropical Pacific based upon satellite-derived cloud water information and moisture profiles. We also examine the relationship between the double ITCZ structure and the underlying sea surface temperature and surface wind fields. Based on the results, we propose a conceptual model for the mechanism of the double ITCZ. Section 2 describes the data and methods, section 3 presents an analysis of these data, and section 4 provides a discussion of the basic mechanisms that determine the structure of the ITCZ in the eastern Pacific. Finally, a summary of the results is given in section 5.

2. Data and methods

For use in climate analyses, the Special Sensor Microwave/Temperature-2 (SSM/T-2) is the only satellite-borne sensor capable of being used to retrieve soundings of tropospheric moisture in cloudy regions. The SSM/T-2 is a five-channel total power microwave radiometer aboard the Defense Meteorological Satellite Program (DMSP) polar-orbiting satellites. This sensor measures the upwelling radiation near the 183.31-GHz water vapor absorption line. The sensor characteristics are listed in Table 1. Many researchers have shown that moisture profiles can be retrieved using radiances measured near the 183-GHz line (Kakar 1983; Lutz et al. 1991; Kuo et al. 1994; Wang et al. 1995). Analysis of cloud water and moisture profile fields retrieved from SSM/T-2 observations (e.g., Wilheit 1990) is extremely limited. The Advanced Microwave Sounding Unit (AMSU), which has been in orbit since 1998, has a sensor (AMSU-B) that is very similar to the SSM/T-2. For climate analysis, its time record (approximately 1 yr at present) is too short and the instrument on board the National Oceanic and Atmospheric Administration's (NOAA) *NOAA-15* is largely unusable, as it has very large scan-dependent biases.

TABLE 1. SSM/T-2 sensor characteristics. The noise equivalent change in brightness temperature (NEdT) is the nominal sensor noise.

Center frequency (GHz)	Side band (GHz)	Half-band width (MHz)	NEdT (K)
91.655	1.25	750.0	0.4
150.000	1.25	750.0	0.5
183.310	1.00	250.0	0.4
183.310	3.00	500.0	0.5
183.310	7.00	750.0	0.6

The presence of atmospheric convection, and hence the ITCZ, is usually inferred by the presence of cloud. Many different types of remote sensing techniques have been used to observe the presence of cloud: solar reflectivity, infrared cloud-top temperature, and liquid water absorption. From these observations, products like outgoing longwave radiation (OLR), precipitation rate, and cloud liquid water (CLW) path are also created, from which many have inferred the presence of convection. None of these observations or products is able to consistently identify the depth of convection. For example, a cold cloud top (low values of OLR) does not necessarily indicate deep convection: it may just be thick cirrus blowoff from nearby deep convection. Similarly, the presence of precipitation or high values of CLW does not necessarily indicate deep convection (the convection may in fact be quite shallow). In order to identify deep convection, the remote sensing technique must account for the presence of high cloud water values throughout the entire column. This is possible if the sensor can be used to retrieve cloud liquid water along with cloud ice water coincident with a nearly saturated column of moist air. The advantage of retrieving both cloud liquid and cloud ice from the same sensor eliminates collocation error as would occur if one were to combine OLR and CLW datasets from different sensors. Furthermore, the presence of cloud liquid and cloud ice retrieved in a single profile ensures that the retrieved profile is radiatively consistent with sensor observations.

A dataset of cloud water path (liquid and ice) and coincident relative humidity profiles produced according to the methods described in Lietzke (1998) was used for this work. The results presented here should not be considered in any way to be validation of the retrieval algorithm used. A comparison to nine radiosonde sites in the Caribbean, over a 2-month period, was completed before application of the algorithm to the eastern Pacific. Table 2 shows the relative humidity profile comparison statistics with the Barbados site where a total of 41 profiles were used. Although this is insufficient to be considered algorithm validation, it is apparent that the

TABLE 2. Relative humidity (%) comparison with the Barbados synoptic radiosonde at retrieved levels.

	0.0 km	1.5 km	3.0 km	5.5 km	7.5 km	9.5 km
Rms (RH%)	7	14	13	15	19	17
Bias (RH%)	−2	−3	1	0	−1	2

retrieved profiles agree with the radiosonde profiles to within about 15%. This is consistent with a retrieval error analysis using simulated radiances that suggested that the rms error was in the 10%–15% range. The analysis of the double ITCZ presented in this paper also relies on the retrieved cloud liquid and ice water paths. It is nearly impossible to validate such retrievals due to the lack of in situ measurements and volume-sampling error. Therefore, although the cloud water plots are given in the appropriate path units of grams per square meter, they should be regarded only as an index of cloud amount, from which relative differences, not absolute quantities, may be inferred.

The SSM/T-2 derived water vapor profiles and cloud water were retrieved twice daily at the sensor's reporting interval (~50 km) and averaged to a 1.0° lat × 1.0° long grid. Since the SSM/T-2 data were obtained from the DMSP *F12* satellite, the earliest observations of the boreal spring are in 1995. The retrievals were limited to the tropical eastern Pacific (15°N–15°S, 75°–165°W) for all reported observations from 1 March to 31 May for the years 1995–97. Surface zonal and meridional winds were obtained from the European Remote Sensing satellite (*ERS-1* and *ERS-2*) scatterometer series. The wind fields were averaged over 6-day periods on a grid of approximately 2.8° lat × 2.8° long (T. Hoar 1998, personal communication). In order to document a longer record of the ITCZ, monthly mean Microwave Sounding Unit (MSU) derived precipitation fields (Spencer 1993) on a 2.5° lat × 2.5° long grid for the years 1982–96 were used. Weekly SST fields (Reynolds and Smith 1995) on 1.0° lat × 1.0° long grids for the years 1982–97 were also used.

3. Results

a. Time evolution

Figure 1 shows a latitude–time plot of monthly mean SST and precipitation averaged over the eastern Pacific (90°–150°W) for the years 1982–97. Consistent with previous studies (e.g., Mitchell and Wallace 1992; Waliser and Gautier 1993), the main precipitation maximum occurs from 5° to 10°N, while a secondary maximum appears briefly, early in the year, near 5°S. We shall refer to the simultaneous occurrence of precipitation maxima on either side of the equator as a ''double ITCZ.'' The double ITCZ undergoes considerable interannual variability; appearing during the boreal spring of some years but not during others. The double ITCZ has been observed to appear as early as late February and disappear as late as early May. However, the most common time period for occurrence is during March and April, which we shall nominally refer to as the boreal spring throughout this paper. The double ITCZ is accompanied by off-equatorial SST maxima (Fig. 1, top), although the position of the southern maximum (5°–10°S) extends a few degrees farther south than its precipitation counterpart. It is apparent that the El Niño–Southern Oscillation cycle, characterized by interannual SST changes in the equatorial eastern Pacific, modulates the double ITCZ structure. The departure from the long-term monthly mean SST averaged over the Niño-3 region is shown in Fig. 2. When SSTs in this region are above normal during the boreal spring, as in 1983, 1987, 1992, and 1997, the double ITCZ is absent; whereas, when they are below normal, as in 1985, 1986, 1989, and 1996, the double ITCZ is prominent.

To help quantify the relationship between the meridional SST profile and the double ITCZ, an index was

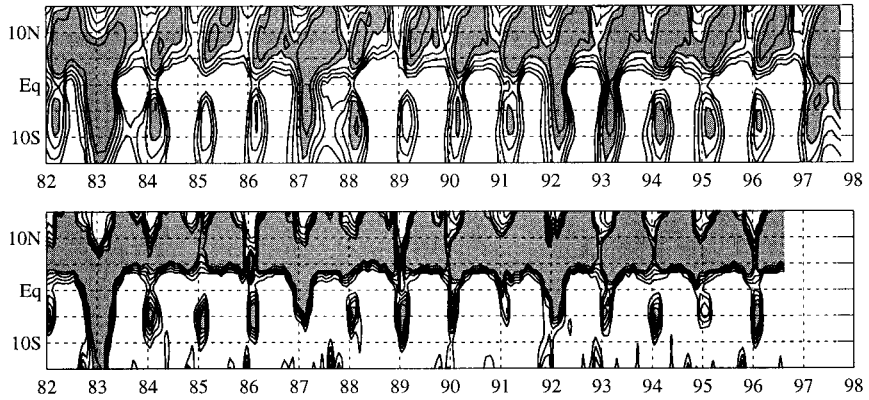

FIG. 1. Latitude–time (Hovmöller) plots of zonally averaged (90°–150°W) monthly mean sea surface (top) temperature and (bottom) precipitation. The SST field is contoured every 0.5°C between 26.0° and 28.0°C with values in excess of 27.5°C shaded. The precipitation field is contoured every 20 mm between 40 and 120 mm with values in excess of 100 mm shaded.

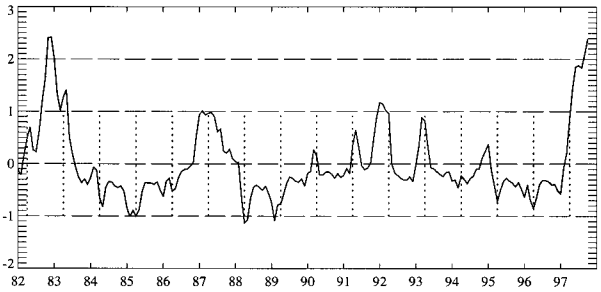

FIG. 2. Niño-3 mean SST departure from long-term monthly mean. Vertical dotted lines denote 1 Apr.

developed to measure the degree of equatorial symmetry present in the precipitation field during any given month. The double ITCZ index, *dI* is defined as

$$dI = \frac{1}{2}[H(5°\text{N}) + H(5°\text{S})] - [H(0°\text{N}) + 1]$$

where

$$H = \begin{cases} 1 & (p \geq 100 \text{ mm}), \\ 0 & (70 < p < 100 \text{ mm}), \\ -1 & (p \leq 70 \text{ mm}), \end{cases}$$

and p is the zonally averaged (90°–150°W) monthly mean precipitation. Using this index, the months when a well-defined double ITCZ was present ($dI = 1$) and the months when no double ITCZ was present ($dI \leq -1$) were identified and are listed in Table 3. Double ITCZ and ''non–double ITCZ'' composites were formed by averaging the SST and precipitation data for all double ITCZ and non–double ITCZ months, respectively. These composites are shown in Fig. 3. During double ITCZ periods (Fig. 3, solid curves), the equatorial minimum in SST is pronounced (SST less than 26°C), while during times when the double ITCZ is absent (Fig. 3, dashed curves), the equatorial minimum is suppressed (SST greater than 27°C). A time series of equatorial SST (not shown) indicates that the SST never exceeds 26.5°C during double ITCZ years, but always exceeds this threshold during years when the double ITCZ is absent. The double ITCZ composite also shows that the SST maxima are located about 3° poleward of the precipitation maxima in both hemispheres. For both sets of composites, the maximum SST is greater in the Northern Hemisphere than in the Southern Hemisphere, while the precipitation profiles are roughly symmetric with respect to the equator. Exclusion of the months January, February, and May from the non–double ITCZ composite has no significant effect on the results (not shown).

TABLE 3. List of months used to composite meridional profiles of precipitation and sea surface temperature for double ITCZ years and non–double ITCZ years.

Double ITCZ years	1982	1984	1986	1988	1989	1993	1994	1996
Mar	X	X	X	X		X	X	X
Apr		X		X	X		X	X
Non–double ITCZ years	1983	1987	1992					
Jan	X							
Feb	X							
Mar	X	X	X					
Apr	X	X	X					
May	X		X					

Having established the general features of the annual cycle and interannual variability of the eastern Pacific double ITCZ and its relation to SST, we now consider in more detail the time evolution of the double ITCZ during the boreal spring. Figure 4 shows weekly means of cloud ice water, cloud liquid water, and SST averaged over the region 90°–150°W, as a function of latitude and time for March–May of 1995 and 1996, both double ITCZ years (recall Fig. 1). Using the retrieved cloud liquid and ice water together, we are able to infer the depth of convection and its dependence on SST. For example, the simultaneous occurrence of cloud liquid and ice water indicates deep convection, while the pres-

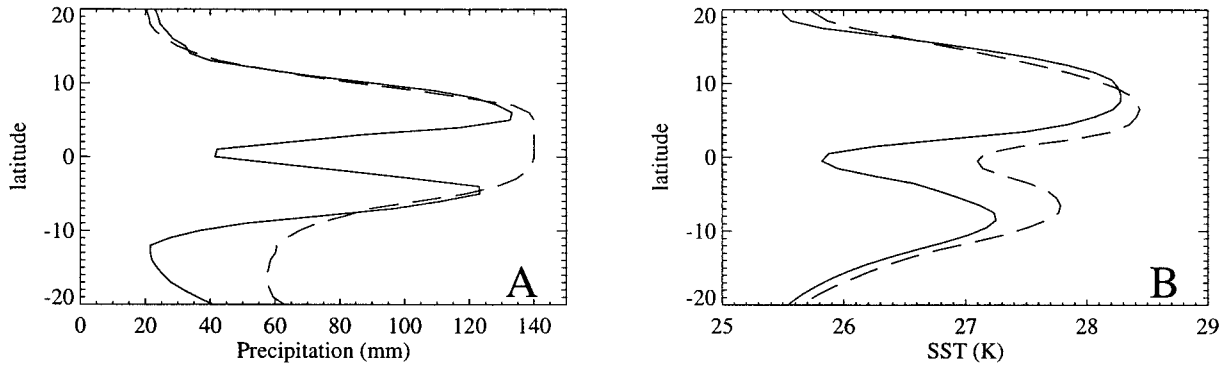

FIG. 3. (a) Composite precipitation and (b) SST for double ITCZ index equal to 1.0 (solid) and for double ITCZ index less than or equal to −1.0 (dash).

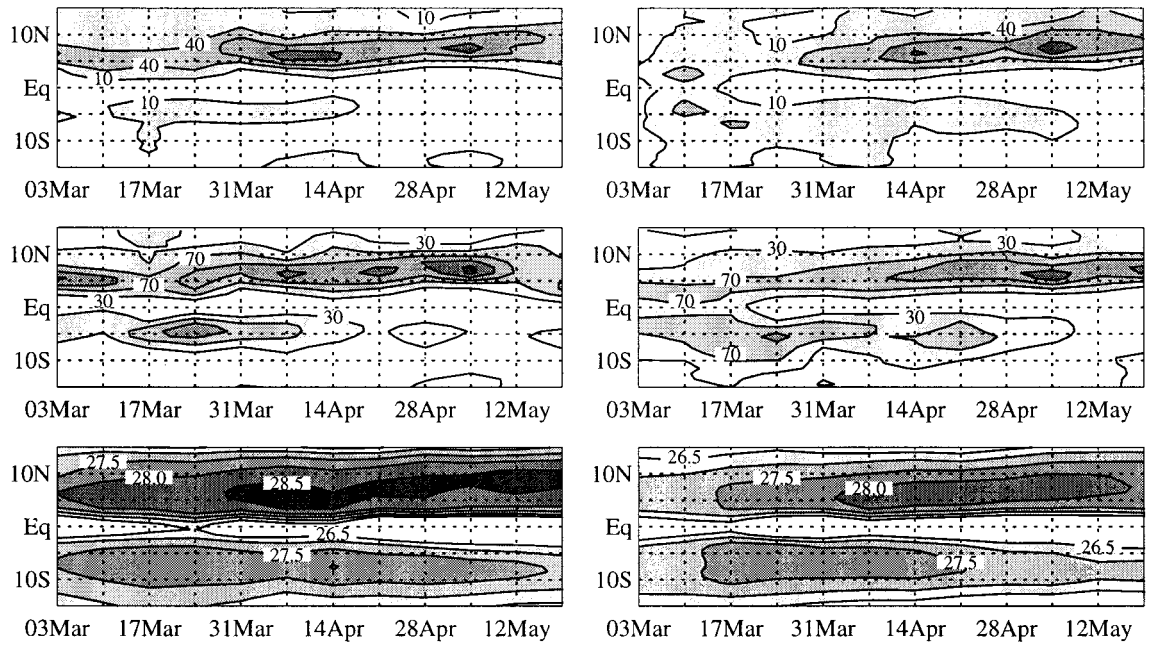

FIG. 4. Latitude–time (Hovmöller) plots of zonally averaged (90°–150°W) weekly mean (top) cloud ice water, (middle) cloud liquid water, and (bottom) sea surface temperature for (left) 1995 and (right) 1996. The cloud ice water field is contoured every 30 g m^{-2} between 10 and 100 g m^{-2} with values in excess of 10 g m^{-2} shaded. The cloud liquid water field is contoured every 40 g m^{-2} between 30 and 150 g m^{-2} with values in excess of 30 g m^{-2} shaded. The SST field is contoured every 0.5°C between 26.5° and 28.5°C with values in excess of 26.5°C shaded.

ence of cloud liquid water alone (cloud ice water alone) indicates low clouds or shallow convection (thick cirrus blowoff from nearby deep convection). During 1995 and 1996, the northern and southern branches of the double ITCZ are marked by the simultaneous occurrence of cloud ice and liquid water. During 1995, the southern branch appears only briefly (10 March–14 April) while during 1996, it is longer lived (3 March–5 May). The appearance of the southern ITCZ during both 1995 and 1996 coincides with the occurrence of a southern SST maximum that is similar in magnitude to the northern SST maximum. The demise of the southern branch of the double ITCZ occurs as the northern branch intensifies with increasing SST.

b. Horizontal structure

The horizontal structure of the double ITCZ as depicted by the cloud liquid and ice water paths is shown in Fig. 5 for the 2-week period immediately following the boreal vernal equinox (23 March–6 April) when the double ITCZ is near its most symmetric state during 1995 and 1996. We will refer to this time interval as the ''double ITCZ period.'' Again, by observing the presence of cloud liquid and ice, we are able to infer the type of convection present. Figure 5 indicates that the southern branch of the double ITCZ in both 1995 and 1996 is of large zonal extent, spanning nearly 70° longitude in both the cloud liquid and ice water fields. In 1997, a partial double ITCZ appears to be present in the ice water field over the western portion of the region, however, the liquid water field does not confirm the double ITCZ structure east of 140°W.

The mean SST and surface wind divergence fields for the double ITCZ period during 1995, 1996, and 1997, are shown in Fig. 6. Comparing the surface wind divergence fields with the cloud ice and liquid water fields (Fig. 5), it is evident that areas of deep convection are accompanied by surface wind convergence maxima ($2–5 \times 10^{-6}$ s^{-1}). The low-level convergence maxima associated with the double ITCZs in 1995 and 1996 tend to occur on the equatorward flanks of the SST maxima in both hemispheres, consistent with the results shown in Figs. 1 and 3. The surface winds overlying the strong equatorial cold tongue in 1996 are divergent. Similar surface wind divergence maps were presented by Zheng et al. (1997) based on ERS-derived winds for 1992–94.

c. Vertical structure

The vertical structure of the relative humidity field can be used to infer vertical motion. In the absence of local moisture sources and sinks and horizontal advection, elevated humidity indicates upward motion (convection), whereas suppressed humidity indicates downward motion (subsidence). The vertical structure of the relative humidity field at 110°W for the double ITCZ period during 1996–97 is shown in Fig. 7. As inferred earlier from the cloud water fields in Fig. 5, the mean latitude and strength of the postequinoctial ITCZ is quite

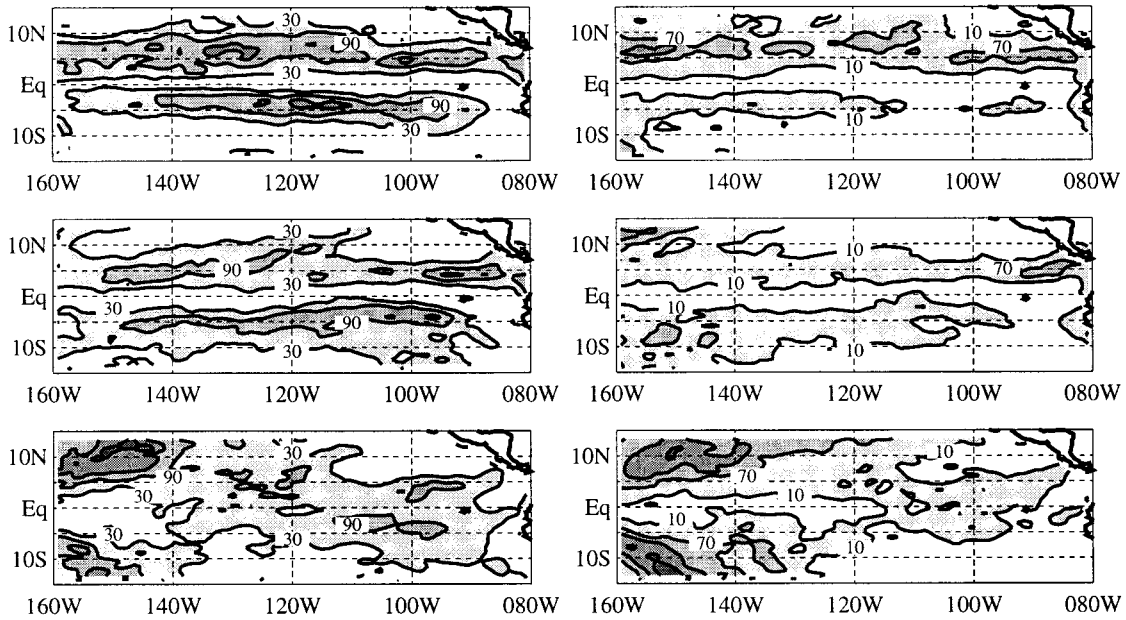

FIG. 5. Time mean (24 Mar–7 Apr) (left) cloud liquid water and (right) cloud ice water for (top–bottom) 1995–97. The cloud liquid water field is contoured every 60 g m^{-2} between 30 and 210 g m^{-2} with values in excess of 30 g m^{-2} shaded. The cloud ice water field is contoured every 60 g m^{-2} between 10 and 190 g m^{-2} with values in excess of 10 g m^{-2} shaded.

different between 1996 and 1997. In 1996, the relative humidity surfaces indicate that upward motion (convection) is present throughout the lower and midtroposphere on either side of the equator, with subsidence at the equator and poleward of 10° latitude. The comparable strength of the inferred upward motion in both branches of the double ITCZ is consistent with the symmetry in the cloud ice and liquid water fields and in the surface wind convergence field shown earlier. The height–latitude relative humidity cross section in 1997 shows no double ITCZ: a single ITCZ is located between 5°N and 5°S with suppressed humidity values on either side (a narrow region of upward motion is also indicated near 12°N).

4. Discussion

The results suggest the following conceptual model of the double ITCZ in the eastern tropical Pacific. The subtropical highs and equatorial trough dominate the large-scale sea level pressure distribution in the eastern tropical Pacific (Fig. 8). During most of the year, the South Pacific high is stronger than its Northern Hemisphere counterpart, extending across the equator and displacing the equatorial trough into the Northern Hemisphere. For a brief period during boreal spring, however, the subtropical highs are symmetrically positioned about the equator. This symmetry produces a region of low-level convergence in the eastern equatorial Pacific at a time when the sea surface is generally warm. Easterly surface winds along the equator produce upwelling that, in the presence of a shallow thermocline, cools the ocean surface mixed layer. The resulting cold tongue along the equator suppresses deep atmospheric convection and splits the convergence zone in two, resulting in a double ITCZ. This phenomenon is observed only during non–El Niño years, and is quite well defined during cold events (La Niña years) when the thermocline is sufficiently shallow to allow the effects of upwelling to impact the heat budget of the oceanic mixed layer. A schematic illustration of an equatorially symmetric double ITCZ circulation with its associated SST profile is shown in Fig. 9a. This situation was present during the cold event of 1996 (recall Figs. 5, 6, and 7). When the sea surface is warmer to the north of the equator than to the south (e.g., in the spring of 1995), convection in the northern branch of the double ITCZ is stronger than that in the south (Fig. 9b). The numerical modeling study of Hack et al. (1989) suggests that the northern ITCZ may act to suppress convection in the southern ITCZ through large-scale subsidence. During El Niño events when the equatorial cold tongue is suppressed (e.g., in 1997), deep convection occurs over the warm sea surface throughout the equatorial region (Fig. 9c).

5. Summary

The present work illustrates how simultaneous retrievals of cloud liquid and ice water and relative humidity profiles from SSM/T-2 radiances can be used to observe the strength and vertical extent of atmospheric convection and large-scale vertical motion. These remotely sensed

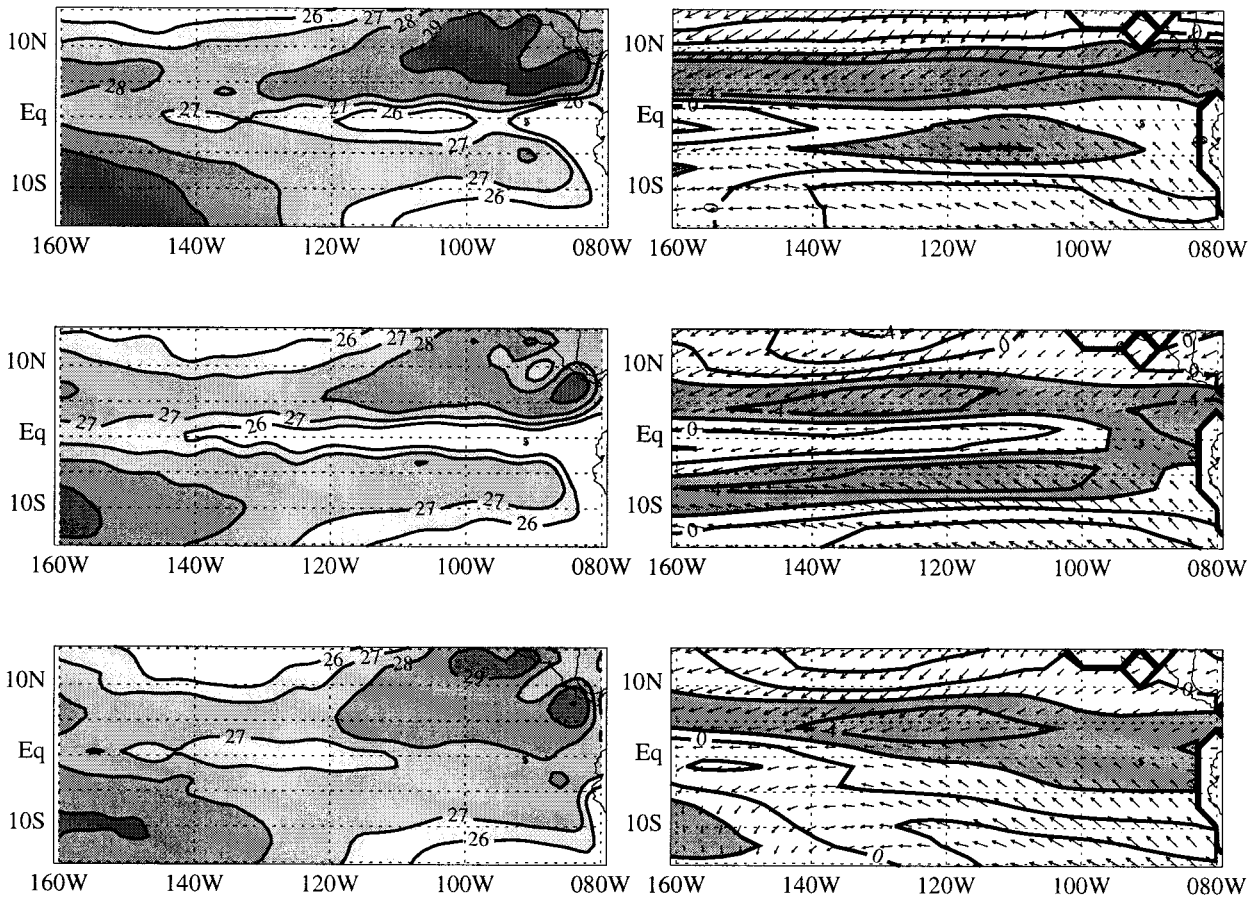

FIG. 6. Time mean (24 Mar–7 Apr) (left) sea surface temperature and (right) surface wind vectors and divergence for (top–bottom) 1995–97. The SST field is contoured every 1°C between 26° and 29°C with values in excess of 26°C shaded. The surface wind divergence field is contoured every 2×10^{-6} s^{-1} between -4×10^{-6} s^{-1} and 4×10^{-6} s^{-1} with values less than -2×10^{-6} s^{-1} shaded.

observations are particularly useful in data-sparse regions like the tropical eastern Pacific. To the best of our knowledge, this study represents the first detailed examination of the three-dimensional structure and temporal evolution of the double ITCZ in the eastern tropical Pacific. The results may be summarized as follows.

1) The double ITCZ, defined by the simultaneous occurrence of deep convection on either side of the equator, is a short-lived phenomenon of approximately 6–8 weeks' duration, present during March and April.
2) Each convective branch of the double ITCZ, located

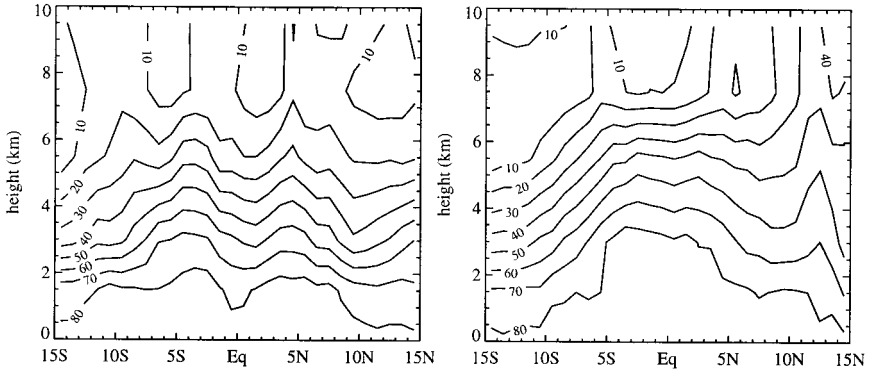

FIG. 7. Time mean (24 Mar–7 Apr) relative humidity height–latitude cross section at 110°W for (left) 1996 and (right) 1997.

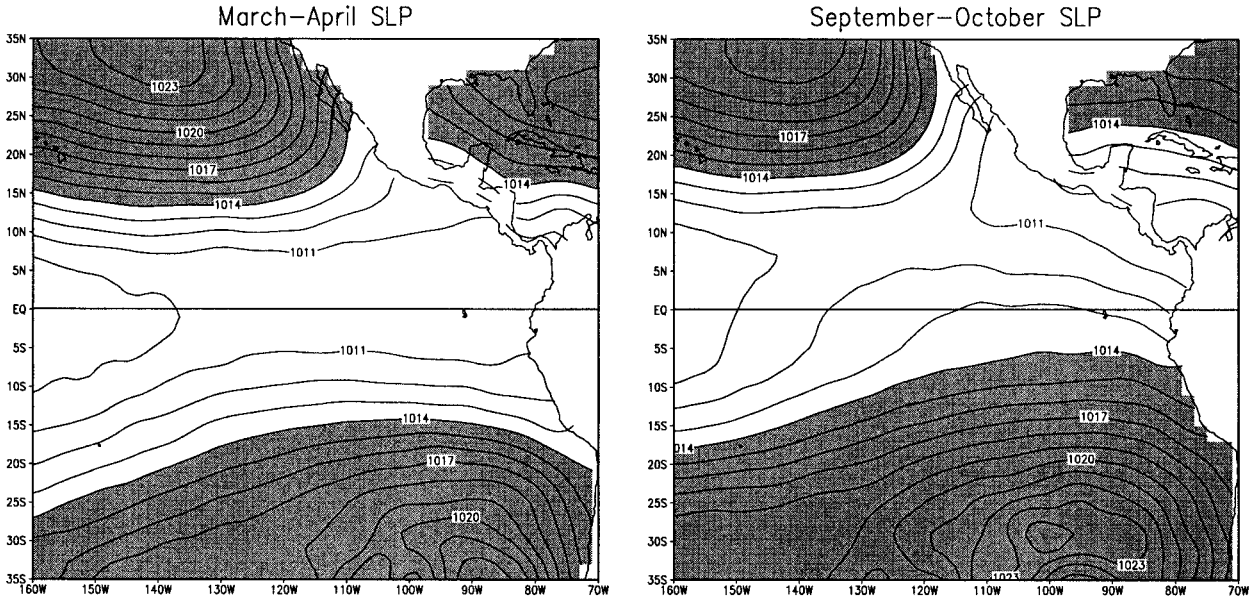

FIG. 8. Comprehensive Ocean–Atmosphere Data Set mean sea level pressure for Mar–Apr and Sep–Oct.

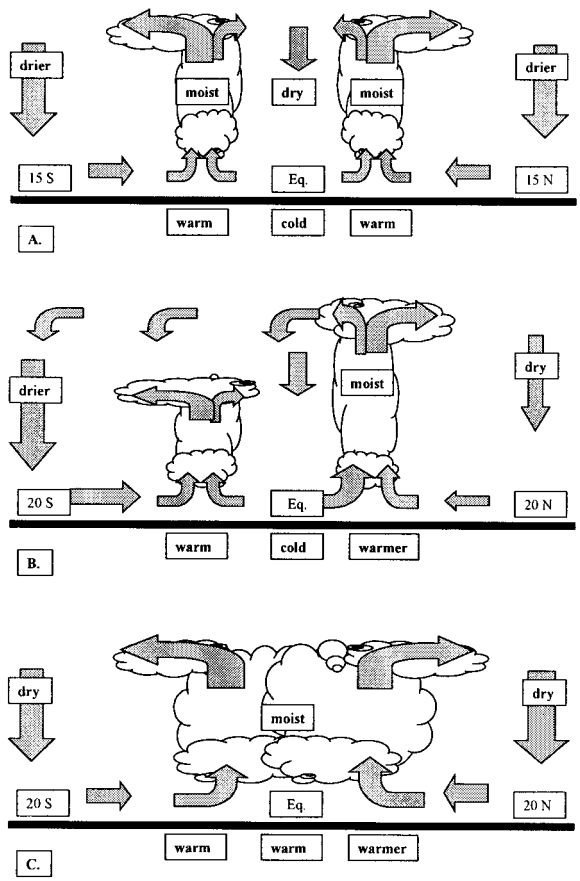

FIG. 9. Illustration of atmospheric motion in the meridional plane for the eastern Pacific ITCZ during the boreal spring of (a) a symmetric meridional SST La Niña year, (b) an asymmetric meridional SST non–El Niño year, and (c) an El Niño year.

near 5°–7° latitude, extends across approximately 70° longitude.

3) The convection and associated upward motion in the double ITCZ is deep, as indicated by the simultaneous occurrence of cloud ice and liquid water as well as by the vertical displacements of relative humidity surfaces throughout the lower and midtroposphere (surface–7 km).
4) Areas of deep convection within the double ITCZ are accompanied by maxima in surface wind convergence. The coincident maxima in convection and surface wind convergence are located several degrees equatorward of the highest sea surface temperatures.
5) The conditions necessary for the formation of a double ITCZ appear to be (a) a general region of low-level wind convergence with a warm sea surface in the deep Tropics, and (b) a narrow sea surface equatorial cold tongue. The former condition occurs every year during March and April, while the latter condition is present during non–El Niño years and is strongest during La Niña years.

Although beyond the scope of this study, it remains to be understood why boreal spring is favored over the boreal autumn for the occurrence of an equatorially symmetric circulation (e.g., a double ITCZ). It is hoped that the present work will stimulate further research of convection and atmospheric vertical motion based on moisture retrievals from the SSM/T-2.

Acknowledgments. We are grateful to the following sources for providing data: NASA Marshall Space Flight Center (SSM/T-2), NOAA Climate Diagnostics Center (MSU Precipitation), and NOAA Climate Pre-

diction Center (SST). The ERS surface winds were provided courtesy of T. Hoar (NCAR). This research was funded by the Center for Geosciences, Phase II at CIRA/CSU under DoD Grant DAAH04-94-G-0420 and by NASA Grant NAG5-3449.

REFERENCES

Charney, J., 1971: Tropical cyclogenesis and the formation of the intertropical convergence zone. *Mathematical Problems of Geophysical Fluid Dynamics,* Vol. 13, *Lectures in Applied Mathematics,* W. H. Reid, Ed., American Mathematical Society, 355–368.

Fernandez-Partagas, J., and M. A. Estoque, 1985: Characteristics of the ITCZ over the eastern Pacific, 5–8 June 1979. *Mon. Wea. Rev.*, **113,** 99–105.

Garcia, O., 1985: *Atlas of Highly Reflective Clouds for the Global Tropics: 1971–1983.* NOAA, Environmental Research Laboratory, 365 pp. [NTIS PB-87129169.]

Gruber, A., 1972: Fluctuations in the position of the ITCZ in the Atlantic and Pacific Oceans. *J. Atmos. Sci.,* **29,** 193–197.

Hack, J. J., W. H. Schubert, D. E. Stevens, and H. Kuo, 1989: Response of the Hadley circulation to convective forcing in the ITCZ. *J. Atmos. Sci.,* **46,** 2957–2973.

Holton, J. R., J. M. Wallace, and J. A. Young, 1971: On boundary layer dynamics and the ITCZ. *J. Atmos. Sci.,* **28,** 275–280.

Hubert, L. F., A. F. Krueger, and J. S. Winston, 1969: The double intertropical convergence zone—Fact or fiction? *J. Atmos. Sci.,* **26,** 771–773.

Kakar, R. K., 1983: Retrieval of clear sky moisture profiles using the 183 GHz water vapor line. *J. Climate Appl. Meteor.,* **22,** 1282–1289.

Kornfield, J., A. F. Hasler, K. J. Hanson, and V. E. Suomi, 1967: Photographic cloud climatology from ESSA III and V computer produced mosaics. *Bull. Amer. Meteor. Soc.,* **48,** 878–883.

Kuo, C. C., D. H. Staelin, and P. W. Rosenkranz, 1994: Statistical iterative scheme for estimating atmospheric relative humidity profiles. *IEEE Trans. Geosci. Remote Sens.,* **32,** 254–260.

Lietzke, C. E., 1998: Satellite moisture profiling of the tropical eastern Pacific convergence zone. Ph.D. dissertation, Colorado State University, Fort Collins, CO, 126 pp.

Lindzen, R. S., 1974: Wave-CISK in the tropics. *J. Atmos. Sci.,* **31,** 156–179.

Lutz, R., T. T. Wilheit, J. R. Wang, and R. K. Kakar, 1991: Retrieval of water vapor profiles from microwave radiometric measurements near 90 and 183 GHz. *IEEE Trans. Geosci. Remote Sens.,* **29,** 602–609.

Ma, C.-C., C. R. Mechoso, A. W. Robertson, and A. Arakawa, 1996: Peruvian stratus clouds and the tropical Pacific circulation: A coupled ocean–atmosphere GCM study. *J. Climate,* **9,** 1635–1645.

Mechoso, C. R., and Coauthors, 1995: The seasonal cycle over the tropical Pacific in coupled ocean–atmosphere general circulation models. *Mon. Wea. Rev.,* **123,** 2825–2838.

Mitchell, T. P., and J. M. Wallace, 1992: The annual cycle in equatorial convection and sea surface temperature. *J. Climate,* **5,** 1140–1156.

Musk, L. F., 1976: Rainfall variability and the Walker cell in the equatorial Pacific Ocean. *Weather,* **31,** 34–47.

Pike, A. C., 1971: Intertropical convergence zone studied with an interacting atmosphere and ocean model. *Mon. Wea. Rev.,* **99,** 469–477.

Reynolds, R. W., and T. M. Smith, 1995: A high-resolution global sea surface temperature climatology. *J. Climate,* **8,** 1571–1583.

Spencer, R. W., 1993: Global oceanic precipitation from the MSU during 1979–91 and comparisons to other climatologies. *J. Climate*, **6,** 1301–1326.

Waliser, D. E., and C. Gautier, 1993: A satellite-derived climatology of the ITCZ. *J. Climate*, **6,** 2162–2174.

——, and R. C. J. Somerville, 1994: Preferred latitudes of the intertropical convergence zone. *J. Atmos. Sci.,* **51,** 1619–1639.

Wang, I. R., S. H. Melfi, P. Racette, D. N. Whiteman, L. A. Chang, R. A. Ferrare, K. D. Evans, and F. J. Schmidlin, 1995: Simultaneous measurements of atmospheric water vapor with MIR, Raman lidar, and rawinsondes. *J. Appl. Meteor.,* **34,** 1595–1607.

Wilheit, T. T., 1990: An algorithm for retrieving water vapor profiles in clear and cloudy atmospheres from 183 GHz radiometric measurements: Simulation studies. *J. Appl. Meteor.,* **29,** 508–515.

Winston, J. S., 1971: The annual course of zonal mean albedo as derived from ESSA 3 and 5 digitized picture data. *Mon. Wea. Rev.,* **99,** 818–827.

Zheng, Q., X.-H. Yan, W. T. Liu, W. Tang, and D. Kurz, 1997: Seasonal and interannual variability of atmospheric convergence zones in the tropical Pacific observed with ERS-1 scatterometer. *Geophys. Res. Lett.,* **24,** 261–263.